

QM/MM Trajectory Surface Hopping Approach to Photoisomerization of Rhodopsin and Isorhodopsin: The Origin of Faster and More Efficient Isomerization for Rhodopsin

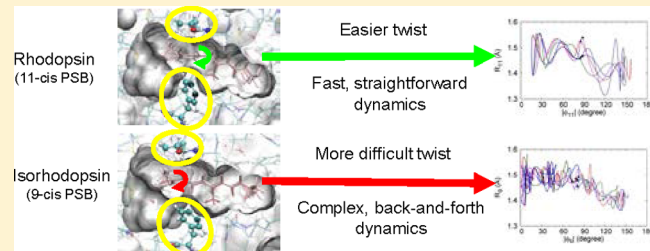
Wilfredo Credo Chung,^{†,§} Shinkoh Nanbu,[‡] and Toshimasa Ishida^{*†}

[†]Fukui Institute for Fundamental Chemistry, Kyoto University, 34-4, Takano-nishihirakicho, Sakyo-ku, Kyoto 606-8103, Japan

[‡]Department of Materials and Life Sciences, Faculty of Science and Engineering, Sophia University, Kioicho, Chiyoda-ku, Tokyo 102-8554, Japan

S Supporting Information

ABSTRACT: The photoinduced *cis*–*trans* isomerization dynamics of rhodopsin and isorhodopsin are studied using a newly developed hybrid QM/MM trajectory surface hopping MD scheme based on the Zhu–Nakamura theory for nonadiabatic transitions. Rhodopsin and isorhodopsin have 11-*cis* and 9-*cis* forms of retinal as chromophore and the two proteins are isomerized to bathorhodopsin enclosing the all-*trans* form. The simulation reproduced faster and more efficient isomerization in rhodopsin than in isorhodopsin. In the excited state, rhodopsin shows a straightforward dynamics, whereas isorhodopsin dynamics is rather complicated and in a back-and-forth manner. The latter complicated dynamics would be mainly due to a narrow space near the active dihedral angle $=\text{C}8=\text{C}9=\text{C}10=\text{C}11=$ (ϕ_9) created by Thr 118 and Tyr 268 in opsin. Rhodopsin gives bathorhodopsin only while isorhodopsin yields a byproduct. The rigorous selectivity in rhodopsin would be another reason why rhodopsin is selected biologically. Comparison with our previous opsin-free investigations reveals that opsin tends to confine the twist of the active dihedral to only one direction and funnels transitions into the vicinity of minimum energy conical intersections (MECI). The twist-confinement totally blocks simultaneous twisting of ϕ_9 and ϕ_{11} ($=\text{C}10=\text{C}11=\text{C}12=\text{C}13=$) and enhances the quantum yields. The opposite rotation of ϕ_9 and ϕ_{11} (“wring-a-wet-towel” motion) takes place upon photoexcitation, which also does without opsin. The wring-a-wet-towel motion is dynamically enhanced in comparison with the one expected from locations of the MECI. The present simulation reveals that the Weiss–Warshel model for *cis*–*trans* photoisomerization is not applicable for rhodopsin because the branching ratio after transition is crucial.



INTRODUCTION

Rhodopsin (Rh) is the photosensitive chemical found on the outer segment of rod-like cells in the retina, the light-sensing structure of the eye.¹ The 11-*cis* retinal chromophore in Rh is changed to an all-*trans* form (now contained in bathorhodopsin) upon exposure of Rh to light.² Bathorhodopsin (bathoRh) is the earliest definitive photoproduct of the Rh photocycle and can be stabilized at low temperatures.^{3,4} Isorhodopsin (isoRh) is an analogue of Rh that contains a 9-*cis* retinal chromophore instead of 11-*cis* retinal embedded in the same opsin environment.^{5,6} The 9-*cis* retinal chromophore in isoRh is converted to the all-*trans* form, which leads to bathoRh formation as Rh does.⁷ In fact, a three-way equilibrium is formed among Rh, bathoRh, and isoRh upon irradiation.^{8,9}

In spite of structural similarity and the same product formation, Rh and isoRh demonstrate quite different rates and efficiencies on photoexcitation. Isomerization of 11-*cis* retinal in Rh to the all-*trans* form is essentially completed in 200 fs,^{10,11} whereas 9-*cis* retinal in isoRh occurs at a longer time scale (600 fs).¹² The isomerization quantum yield in Rh was reported to be 0.67 by Dartnall et al.¹³ and 0.65 by Kim et al.,¹⁴ but in

isoRh, a reduced quantum yield (0.22)¹⁵ was observed, which results in a weaker visual response.¹⁶ Hurley et al. examined the temperature and wavelength effects on the photochemistry of Rh, isoRh, and bacteriorhodopsin and their photoproducts.¹⁵ The absence of temperature and wavelength dependencies of Rh bleaching was attributed to a *cis*–*trans* isomerization that takes place after thermal relaxation, where no activation energy is required. On the other hand, the isoRh → bathoRh isomerization showed temperature and wavelength dependence at 77 K. It was proposed that this was due to a small barrier along the potential energy surface in the excited state. The large differences in reaction time scale and quantum yield, despite a small structure difference and the generation of the same product for Rh and isoRh, makes the comparative study of the two species very attractive to better understand the processes involved in the initiation of visual recognition.

Received: December 22, 2011

Revised: June 11, 2012

Published: July 11, 2012

Schoenlein et al. suggested, on the basis of the Landau-Zener description, that the slower reaction time and the lower yield in isoRh were due to slower speeds along the reaction (twist) coordinate in the curve crossing area.¹² Okada et al. reported the X-ray structures of Rh, which showed that the twist angles at the *cis* position, ϕ_{11} dihedral, was twisted by 38° in the counterclockwise direction inside the protein binding pocket¹⁷ and by 15° for ϕ_9 in isoRh.¹⁸ (The dihedral angles of the carbon backbone will be designated as “ ϕ_n ”, which refers to the torsion angle C(n-1)-C(n)-C(n+1)-C(n+2), for example, ϕ_9 is the twist angle of C8-C9-C10-C11. The notation does not imply any bond order of the atoms involved. Hereafter, we call ϕ_{11} in Rh and ϕ_9 in isoRh active angles because the angles are twisted in the isomerization.) They claimed that the twist is due to the surrounding protein.¹⁸ They also attributed the larger twist in Rh mainly to the steric repulsion between the C13 methyl group and C10 hydrogen.¹⁷ They proposed that this significant pretwist is responsible for Rh's highly efficient isomerization.¹⁸ Sekharan et al. argued the assistance of photoisomerization by repulsive interaction of the retinal chromophore with the surrounding protein from X-ray analysis and quantum-mechanical calculations.¹⁹

Hayashi and co-workers²⁰ carried out a CASSCF(12,12)/DZP/Amber QM/MM molecular dynamics calculation of the photoisomerization dynamics of Rh. Their calculation revealed a dynamically homogeneous excited-state dynamic that resulted in an ultrafast photoisomerization due to weak perturbations of the surrounding protein, but they did not estimate the quantum yield as they neglected contributions from trajectories surviving in the excited state after passing the curve-crossing region. In another QM/MM MD simulation, a single-trajectory calculation using a scaled CASSCF/6-31G*/Amber potential that is designed to reproduce a CASPT2//CASSCF/6-31G*/Amber potential energy profile was done by Frutos et al.²¹ for Rh. It was revealed that the conical intersection is reached within 110 fs via a space-saving asynchronous (so-called) bicycle-pedal or crankshaft motion of the retinal backbone, but only one trajectory was calculated and the transition and the dynamics in the ground state were not considered.

In one of our previous work, classical dynamics calculations based on ab initio quantum chemical calculations was carried out to probe the nonadiabatic photochemical dynamics of two model systems of the protonated Schiff base (PSB) of 11-*cis* retinal in the gas phase.²² The Zhu-Nakamura formulas were employed to estimate the probability of nonadiabatic transition between the electronically lowest excited and ground states. The twist in the opposite direction of the ϕ_9 and ϕ_{11} dihedrals was found to be intrinsic to the chromophore and not induced by the surrounding protein. In the other of our work on model PSB of 9-*cis* retinal,²³ it was suggested then that a 10 kcal mol⁻¹ barrier in the excited state of 9-*cis* retinal slows down the photoisomerization dynamics and makes it less efficient due to premature transitions far from the minimum energy conical intersection (MECI). In spite that the pretwist was not included in this gas-phase calculation, we reproduced the differences in quantum yield and reaction time qualitatively. Thus, we claimed that pretwist was not the main reason for the differences. (We shall refer to these two sets of opsin-free simulations as the “PSB calculations” or “opsin-free calculations” hereinafter.)

Strambi et al. performed reaction path searches for Rh and isoRh²⁴ and argued the relationship of relaxation in the excited state between the two biomolecules. They employed a

dynamically correlated QM method, but no dynamics calculation was done. They left two open questions for the photoinduced isomerization. The more fundamental one of the two is what the molecular factor is at the basis of the higher quantum yield of Rh than isoRh.

In this paper, we extend the study of photoinduced *cis-trans* isomerization of Rh and isoRh by including the effects of the opsin environment. To achieve this goal, we combined the Zhu-Nakamura trajectory surface hopping scheme with Morokuma's ONIOM^{25,26} method. Here, we chose the QM/MM variety where the high-level layer is treated quantum-mechanically, whereas molecular mechanics model chemistry is used for the low-level layer, where we designed a set of opsin-free and opsin-enclosed calculations so as to compare the present results with our previous calculations. The result is a novel scheme we shall refer to from here on as a ZN-QM/MM-TSH scheme. To our knowledge, this is the first time such a hybrid scheme is employed although other TSH schemes have been combined with the QM/MM method in the past.^{20,27-33} Tully's fewest switches surface hopping (FSSH) is often used for TSH treatment.^{34,35} FSSH directly use the information of electronic structure propagated. The present scheme, on the other hand, uses only the information of the relevant adiabatic potential energy surfaces (PES) for hopping decisions (indirectly including electronic structure information via PESs).

We have reported some of the present results in a letter article³⁶ and argued mainly the reason why life chooses Rh, not isoRh. This paper will deal with dynamics in Rh and isoRh in a much more comprehensive manner and comparison with our previous calculations in vacuo in details.

We will discuss applicability of the *cis-trans* photoisomerization model proposed by Weiss and Warshel in 1979.³⁷ In their model, the active twist angle oscillates around the crossing region in the excited state and the direction of the twist angle momentum uniquely determines products. The quantum yield stems mainly from the transition probability per passing through the crossing region. The present simulation for Rh, however, will reveal that the branching ratio after transition plays a crucial role, whereas the Weiss-Warshel model assumes that the ratio is unity.

CALCULATIONS

On-the-fly classical molecular dynamics calculations combined with hybrid QM/MM computations were carried out where nonadiabatic transitions were taken into account. The QM/MM treatment was done by the ONIOM scheme using the mechanical embedding treatment in Gaussian 03.³⁸ The QM treatment employed state-averaged complete active space self-consistent field³⁹ (CASSCF) ab initio quantum-mechanical techniques. The CASSCF calculations used six electrons in six orbitals for the active space (CASSCF(6,6)) with the 6-31G basis set⁴⁰ and the two lowest states are averaged. All the active orbitals have π character. The MM part was described by AMBER parameters collectively known as parm96.dat force field,⁴¹ as implemented in Gaussian 03.

The QM region coincides exactly with the PSB of retinal where two methyl groups at position 1 were removed as were done in the PSB calculations (see Figure 1, ref 1 and Figure 2, ref 2). This was done intentionally so that new observations can be attributed solely to the surrounding protein. The rest of the molecule of Rh or isoRh was treated with the AMBER molecular mechanics force field.

The velocity Verlet algorithm⁴² was used to calculate trajectories of nuclear motion. In the present treatment, no restrictions for symmetry or orbital occupations are placed when the six active orbitals are chosen. It is known that a CASSCF treatment of retinal overestimates bond alternation, torsion-angle between the backbone and the β -ionone ring, and excitation energy.¹⁹ However, the bond alternation and the torsion angle are qualitatively reproduced. We chose the present level for the electronic structure part as a compromise between reasonable descriptions of dynamics and computational feasibility. It typically took 7 weeks for one trajectory on our Intel Core 2 machine with a clock of 2.66 GHz although we employed a variety of machines.

The initial geometry is the optimized ground state geometry and the initial atomic velocity was generated at $T = 300$ K and the molecule was excited onto the S_1 state. A total of 162 trajectories were calculated in total for both Rh and isoRh with a 0.5 fs time step. The surface hopping procedure is based on the Zhu–Nakamura theory,^{43–47} which provides a complete set of solutions for the curve-crossing problem, covering the whole energy range. The details of the procedure is described previously.^{22,23}

Generation of each product is counted only after one of product regions in the ground state is reached. The quantum yield or reaction probability Φ , computed within one standard deviation for the mean, is calculated using the formula⁴⁸

$$\Phi = \frac{N_R}{N} \left(1 \pm \sqrt{\frac{1}{N-1} \left(\frac{N}{N_R} - 1 \right)} \right)$$

where N is the total number of trajectories and N_R is the number of reactive trajectories.

RESULTS AND DISCUSSION

Energetics of the Systems. In this study, two rotation centers ($-C_9=C_{10}-$ and $-C_{11}=C_{12}-$) are closely monitored and Rh isomers are classified according to the torsion angle adapted by these rotation centers giving rise to four isomeric species: Rh, isoRh, bathoRh, and a 9,11-di-*cis* isomer, which contains 11-*cis*, 9-*cis*, all-*trans*, and 9,11-di-*cis* isomers of retinal chromophore, respectively. (We call the last isomer as 9-11-di-*cis* rhodopsin (9,11-di-*cis*-Rh) hereafter.) Figure 1 shows an energy diagram for the ground state (S_0) and the first excited state (S_1) potential energy spanned by these

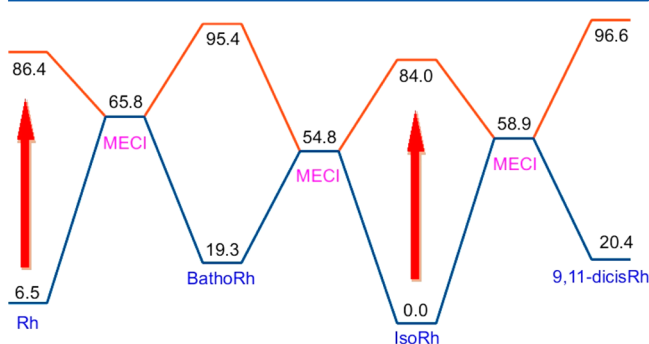


Figure 1. Energy diagram for the *cis-trans* isomerization of Rh and isoRh. Energy is in kcal mol^{-1} . The blue and red lines indicate the ground and excited states, respectively. MECI = minimum energy conical intersection. The energy for an MECI is the average of the energies of S_1 and S_0 .

four isomers (see also, Figure S1 in Supporting Information (SI) for comparison with the corresponding system in vacuo).

Ground-State Energies. Our calculations reveal that isoRh is the most stable isomer within the set, whereas the 9,11-di-*cis*-Rh is the most unstable in the ground state. The order of relative energies, $E(\text{bathoRh}) > E(\text{Rh}) > E(\text{isoRh})$, is in agreement with the order reported by Yoshizawa and Wald's⁷ spectroscopic measurements, whereas Schick⁸ reported the order in enthalpy at 77 K more recently: $H(\text{bathoRh}) > H(\text{isoRh}) > H(\text{Rh})$. This difference in the relative stability of Rh and isoRh from the measurement of Schick et al. would not influence dynamics significantly because we treat photo-excitation and the excitation energy is qualitatively reproduced, as shown later. The relative ground-state energies of the retinal isomers in vacuo (11-*cis* > 9-*cis* > all-*trans*; see Figure 1, ref 2, or Figure S1, SI) were different from those in opsin environment (bathoRh(all-*trans*) > Rh(11-*cis*) > isoRh(9-*cis*)).

The direction and the relative magnitude of the pretwist is in agreement with X-ray observations,^{17,18} as shown in Table 1. The ϕ_{11} in Rh and ϕ_9 in isoRh's are -17.9 and -6.3° , which qualitatively reproduced the angles of -38 and -15° , determined by the X-ray analysis, respectively.^{17,18} One may attribute the difference of the reaction times and quantum yields to the difference in the pretwist, but this is not the main reason, as referred to in the Introduction and discussed in detail in our previous paper.²³ For the bathoRh equilibrium geometry, large deviations of $\phi_9 = -150^\circ$ and $\phi_{11} = -154^\circ$ from the perfect *trans* configuration ($\phi = -180^\circ$) are also in agreement with X-ray crystallography results of $\phi_9 = -156^\circ$ and $\phi_{11} = -154^\circ$.⁴⁹

Excitation Energies. The present calculation gave excitation energies between 76 and 84 kcal mol^{-1} , which overestimated experimental measurements in the range of 53 to 59 kcal mol^{-1} (543–483 nm), as shown in Table 1. The overestimation would be due to the of the CASSCF method.¹⁹ Nevertheless, the relative order of the vertical excitation energies (isoRh > Rh > bathoRh)^{7,24,50–52} is qualitatively duplicated. The qualitative replication of the relative excitation energies should be sufficient for our purpose. Without the protein, the order of the excitation energy was 9-*cis* (isoRh) > all-*trans* (bathoRh) \sim 11-*cis* (Rh),^{22,23} where the corresponding protein is shown in parentheses. The changes of excitation energy order would be partially due to the MM force field treatment because, in the present calculations, the same MM force fields employed for the ground state as well as the excited state. The force field description in the excited state would be worse because the force field was determined in the ground state.

Minima in S_1 . An extensive search for the minimum in the excited state were done, but no minimum was found. Strambi suggested one around $\phi_9 = -50^\circ$ for the counterclockwise pathway from isoRh to MECI(isoRh \rightarrow bathoRh).²⁴ In our previous calculation in vacuo, we found a one.²³ The lack of S_1 minima will be discussed later.

MECI. The ground and first excited state surfaces are interconnected by conical intersections at which the geometry involves a twist to about halfway between *cis* and *trans* configurations in one rotation center. Table 2 shows the dihedral angles ϕ_9 and ϕ_{11} at MECIs. Because the energy difference is not converged to less than 1.0 kcal mol^{-1} after several attempts for conical intersection searches, the averaged energies are shown in Table 2 and Figure 1. Among the three MECIs, the order of the energy of MECI is MECI(Rh \rightarrow bathoRh) > MECI(isoRh \rightarrow 9,11-di-*cis*-Rh) > MECI(isoRh \rightarrow

Table 1. Relative Energies, Dihedral Angles ϕ_9 and ϕ_{11} , and Excitation Energies at Minima in the Ground State^a

	Rh(11-cis)		bathoRh(all-trans)		isoRh(9-cis)		9,11-di-cis-Rh
	QM/MM ^b	expt	QM/MM ^b	expt	QM/MM ^b	expt	QM/MM ^b
relative S_0 energy (kcal mol ⁻¹)	6.5 [5.4]	2.0, ⁷ -5.1 ⁸	19.3 [-0.5]	5.9, ⁷ 27.1 ⁸	0.0 [0.0]	0.0 ^{7,8}	20.4
ϕ_9 (deg) ^c	173.9 [180.0]	-176.0, -176.4 ¹⁷	-150.2 [179.9]	-154.2, -152.7 ⁴⁹	-6.3 [0.1]	-12.3, -18.7 ¹⁸	23
ϕ_{11} (deg) ^c	-17.9 [0.5]	-40.8, -36.1 ¹⁷	-154.2 [-180.0]	-155.8, -157.4 ⁴⁷	173.4 [-179.9]	166.9, 166.4 ¹⁸	27.3
excitation energy (kcal mol ⁻¹)	80.0 [82.3]	56.5-57.4 (498-506 nm) ^{7,10,50-52,66,67}	76.1 [82.4]	52.7-53.4 (535-543 nm) ^{7,10,50-52}	84.0 [83.2]	57.9-59.2 (483-494 nm) ^{7,50-52,67}	76.3

^aThe values in square brackets are the ones from the corresponding gas-phase PSB calculations (refs 1 and 2). Reference of energy is taken to be the energy in the ground state (S_0) for isoRh. ^bCASSCF(6,6)/6-31G/Amber. ^cPositive/negative sign indicates the dihedral angle is twisted in the clockwise/counterclockwise direction.

Table 2. Relative Energy Differences and Dihedral Angles at the Minimum Energy Conical Intersection Points (MECI)^a

	Rh → bathoRh		IsoRh → bathoRh		IsoRh → 9,11-di-cis-Rh
	Present	Strambi et al. ^b	Present	Strambi et al. ^b	Present
Relative S_0 energy (kcal mol ⁻¹)	65.8 ^d [68.0]	37.1 ^d	54.8 ^d [50.6]	40.1 ^d	58.9 ^d
ϕ_9 (deg)	-161.6 [-178.8]	-161	-89.7 [-91.9]	-90	23.7
ϕ_{11} (deg)	-91.4 [-93.7]	-80	-162.7 [-179.6]	-155	101.4

^aThe values in square brackets are those in the gas phase calculations.^{22,23} ^bReference 24. ^cRelative S_0 energy from the minimum in the ground state for isoRh. ^dThe average energy of S_1 and S_0 .

bathoRh). Strambi et al.²⁴ reported that, using dynamically correlated techniques and a larger active space, the MECI(Rh → bathoRh) was lower than MECI(isoRh → BathoRh). In the vacuo calculations, MECI(11-cis → all-trans) is also lower than MECI(9-cis → all-trans).^{22,23} In all cases, at MECIs, the double bond within the active torsion coordinate is stretched to a single bond.

We carried out exhaustive search for an MECI that connect isoRh PES to the bathoRh PES involving a clockwise twist in $-C9=C10-$, but did not find one. The same is true in the Rh → bathoRh case wherein the geometry at the conical intersection involves a large twist in the $-C11=C12-$ coordinate. This is in contrast with our previous calculations in vacuo, where we found the MECIs.^{22,23}

In our previous PSB calculation, we found an MECI that directly connects the ground state 9-cis and 11-cis forms²² (see Figure 2a, ref 1). The MECI, however, disappears when the opsin environment is taken into account as the present QM/MM calculation failed to locate this MECI. It will be shown later that photoexcitation of Rh does not produce isoRh (and vice versa). Consistent with the PSB calculation in vacuo, the MECI(Rh → bathoRh) lies above the MECI(isoRh →

bathoRh) although inclusion of the opsin residues as an MM field reduces the energy difference by 6.4 kcal mol⁻¹.

At the MECI points, the active dihedrals are twisted to around -90° except for the isoRh → 9,11-di-cis-Rh case, where ϕ_{11} is some 11° off from the expected twist angle of 90° . The energy difference between the excitation energy in Rh and the MECI(Rh → bathoRh) (20.6 kcal mol⁻¹) is smaller than the corresponding energy difference (29.2 kcal mol⁻¹) between the excitation energy in isoRh and the counterpart MECI, MECI(isoRh → bathoRh). The present result is in qualitative agreement with the excess energies obtained by Strambi et al. of 15 and 22 kcal mol⁻¹ for Rh and isoRh²⁴ based on a more sophisticated QM method. The excess energy for Rh would therefore be smaller than that for isoRh in the region where transitions to the ground state take place. Thus, the difference in excess energy would not be the origin of the difference in rate and efficiency between Rh and isoRh.

The twists of the ϕ_9 in Rh and ϕ_{11} in isoRh are accompanied with the rotations in the opposite direction of the active angles ϕ_{11} and ϕ_9 in the 11-cis and 9-cis retinal chromophore in the respective proteins. The ϕ_9 in Rh and ϕ_{11} in isoRh are twisted clockwise by 18.4 and 17.3° , respectively, from the in vacuo values, which are consistent with the QM/MM result by Strambi et al.

Effects of the Opsin Environment. The relative ground-state energies of the retinal isomers in vacuo were different from those in opsin environment, but this is not quite surprising since relative energies are largely subject to space constraints by the opsin environment. Destabilization of the all-trans form has been reproduced correctly although the order of energies of Rh and isoRh is different from the experimental order determined experimentally.⁸ The order of the relative excitation energies is likewise corrected with the addition of the opsin environment in spite of overestimation. The theoretical excitation energy would be more sensitive to the choice of level of QM theory, basis set, and size of the active space rather than to the explicit consideration of the surrounding amino acids.

The MECI for Rh → bathoRh isomerization lies above the isoRh → bathoRh MECI, which is in agreement with the previous calculation in vacuo,^{22,23} whereas the dynamically correlated level with a larger active space calculation by Strambi et al.²¹ gave the opposite order. Again, we expect this quantity

to be more sensitive to the quantum chemical parameters rather than inclusion of the opsin environment.

Unlike that in the gas-phase study of 9-*cis* retinal, no energetic barrier is found in the excited state of isoRh. Thus, the 10 kcal mol⁻¹ barrier in the PSB simulation²³ may be an artifact caused by the disregard of the effects of the opsin environment. The disappearance of the barrier may be partially due to the less appropriate treatment of MM force field in the excited state, as the MM force is determined for the ground state. If any barrier does exist, it would be very low and be extremely elusive in the geometry optimization in a huge dimensionality of the QM/MM space. The disappearance (or lowering) of the excited-state barrier is consistent with the assertion of Birge et al.⁵³ that the opsin environment lowers the activation energy in the excited state.

In the gas-phase PSB model study, the PES shows strong bidirectional properties. That is, the PES shows that the products can be accessed in either twist direction of the active coordinate. We found two MECIs that connect the 9-*cis* PES with that of the all-*trans* isomer, one each for the clockwise and counterclockwise twist of the C9=C10 dihedral. The same was true for the 11-*cis* → all-*trans* case. In the present opsin-enclosed calculation, however, we have found only the MECIs in which the active dihedral is twisted counterclockwise. This difference in the PES feature is presumably due to the hindrance offered by the amino acid residues that surround the chromophore.

CAS Space and Mechanical/Electronic Embedding. One may consider that the present CASSCF(6,6) calculations with mechanical embedding (ME) is not enough to describe the dynamics reasonably because of its small space of CAS and neglect of charge effects from opsin. We evaluated the excitation energies for Rh and isoRh at the CASSCF(12,12) level with electronic embedding (EE) at the initial geometries, which is the optimized geometries at the CASSCF(6,6) level. The excitation energies for Rh and isoRh were 72.2 and 78.3 kcal mol⁻¹, which were less than the present values of 80.0 and 84.0 kcal mol⁻¹ but still significantly overestimated the experimental values of 57–59 kcal mol⁻¹. On the other hand, one time step calculation at the CASSCF(12,12)-EE was found to be about 2.5 times more expensive than CASSCF(6,6)-ME, which means that it would take 4–6 months to calculate one trajectory. Thus, the present CASSCF(6,6) would be a reasonable compromise between accuracy and feasibility.

Overall, the calculated PES is in qualitative agreement with the experimental measurements and, thus, we are confident that we should be able to simulate a reasonably accurate dynamics of the system at the chosen level of approximation.

Quantum Yields. Table 3 shows the ratio of photoproducts, quantum yield and photoisomerization period. The bathoRh quantum yields are 0.52 and 0.31 for Rh and isoRh, respectively. The corresponding experimental values are 0.65 and 0.22.^{14,15} Thus, the present simulation reproduced the experimental fact that the yield from Rh is larger than that from isoRh. The yield from isoRh is slightly overestimated compared to that of the experimental quantum yield. This overestimation may be due to the underestimation of the disturbance by the opsin environment and irreproducibility of the S₁ barrier.

In the gas phase PSB simulation, production of the all-*trans* photoproduct was only 13 and 27% from the 9-*cis* and 11-*cis* starting materials, respectively. Thus, generation of bathoRh from both isoRh and Rh is approximately doubled compared to that revealed in the opsin-free calculation.

Table 3. Ratio of Photo Products, Quantum Yield, and Photoisomerization Period of Rhodopsin in Comparison with Isorhodopsin^a

		reactants	
		Rh(11- <i>cis</i>)	isoRh(9- <i>cis</i>)
photoproducts (%)	bathoRh(all- <i>trans</i>)	52 [27]	31 [13]
	isoRh(9- <i>cis</i>)	0 [22]	65 ^b [82]
	Rh(11- <i>cis</i>)	48 [51]	0 [5]
	9,11-di- <i>cis</i> -Rh	0 [0]	4 [0]
quantum yield	calcd	0.52 [0.27]	0.31 [0.13]
	expt	0.65 ¹⁴	0.22 ¹⁵
photoisomerization period	calcd	187 fs [185 fs]	344 fs [665 fs]
	expt	200 fs ^{10,11}	600 fs ¹²

^aThe values in square brackets are taken from the corresponding gas-phase PSB calculations.^{22,23} ^bA total of 56% of the total trajectories are generated from an initial counterclockwise twist of ϕ_9 and a clockwise twist of ϕ_{11} , and the twists in the opposite directions after transitions near the MECI(isoRh-bathoRh), whereas 9% comes from an initial clockwise twist of ϕ_9 and a counterclockwise twist of ϕ_{11} , and the twists in the opposite directions after transitions near the MECI(isoRh-9,11di-*cis*-Rh). In total, 65%.

Polli and co-workers²⁷ used a larger active space (CASSCF-(10,10)) and polarization on chromophore heavy atoms (6-31G*) in a QM/MM trajectory surface hopping simulation of the Rh photoisomerization. They calculated 38 trajectories and obtained a quantum yield of 0.61, which is closer to the experimental value of 0.65 than what we report. We should, however, mention that we used 162 trajectories to come up with our conclusions. As a trial, we took out the first 38 trajectories from the whole set and analyzed them as usual. We discovered that the statistics given by the subset is very different from those obtained using the whole set. This small experiment leads us to wonder if 38 trajectories would be enough to yield a statistically representative result.

Photoexcitation of Rh leads to only bathoRh and the reactant, and thus generation of isoRh is totally blocked by the opsin environment as is expected.⁵⁴ The regeneration ratio of Rh is almost the same both in the present simulation (48%) and the gas phase one (51%). Thus, we can have a rough picture that the trajectories that would produce the 9-*cis* products without the opsin environment are actually blocked away to generate the all-*trans* product bathoRh instead.

The opsin in isoRh, on the other hand, suppresses the regeneration of the reactant (82% in the gas phase PSB calculation compared to 65% in this simulation) and favors production of bathoRh instead (from 13% to 31%). In the gas-phase simulation of the photoisomerization of the PSB of 9-*cis* retinal, 5% of the product generated was the 11-*cis* isomer involving simultaneous but asynchronous isomerization of the 11-position. When the opsin environment is taken into account, production of the doubly twisted product, Rh, is totally eliminated (from 5% to naught) as it is also the case above for Rh → isoRh (from 22% to naught). Thus, it is found the opsin environment totally blocks simultaneous twisting of ϕ_9 and ϕ_{11} for Rh as well as isoRh while the twist in the opposite direction of ϕ_9 and ϕ_{11} can be seen in all the cases as shown later. Schick et al. and Hug et al. proposed a three-way equilibrium among Rh, bathoRh, and isoRh upon irradiation.^{8,9} The present result

indicates that the equilibration between Rh and isoRh is not direct and is through bathoRh.

Photoexcitation of isoRh yields a small portion of 9,11-di-*cis* product (4%) in addition to bathoRh as products, whereas Rh gives the bathoRh alone. Trehan et al. found that the 9,11-di-*cis* product was formed from the interaction of 9-*cis* and 11-*cis* retinal with bovine opsin,⁵⁵ although the product has not been reported in photoexcitation of isoRh to the best of our knowledge. The rigorous selectivity of photoproducts for Rh would be another biological reason for living creatures to choose Rh rather than isoRh. It would be highly desirable to give only one product for accurate functioning of an organ when the trigger reaction happens. IsoRh gives a byproduct of 9,11-di-*cis*-Rh, although the ratio is not very high, which would disturb an accurate functioning if isoRh was used for photovision.

Reaction Time and Population Change with Time. The temporal change of the population of the photoproducts and residual reactant in this simulation is shown in Figure 2 (see also Figure S2 for comparison with the in vacuo counterparts, SI). The well-established isomerization period of Rh and isoRh is 200 fs^{10,11} and 600 fs,¹² respectively, measured by femtosecond pump–probe spectroscopy. At this time scale,

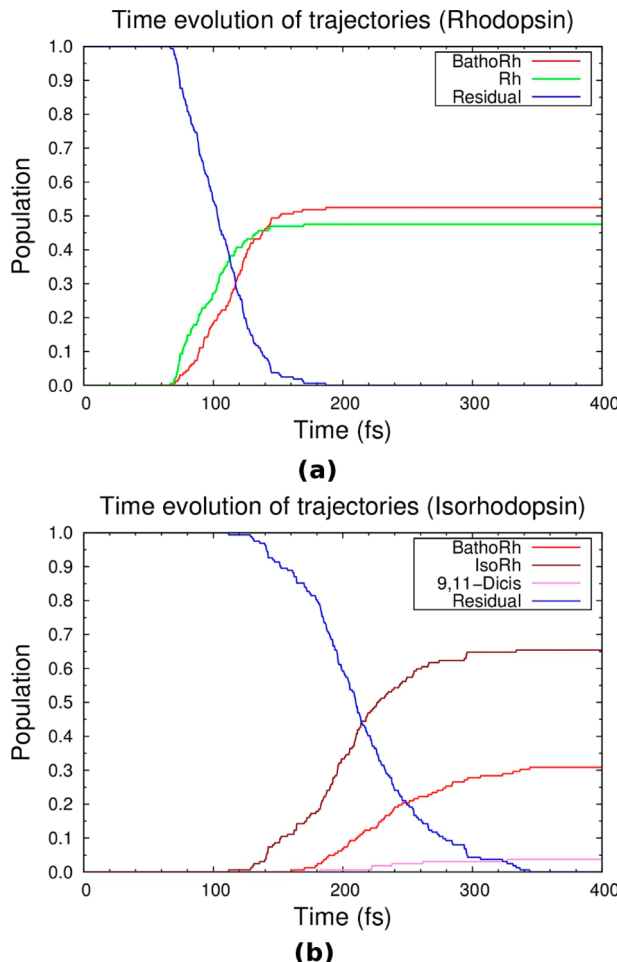


Figure 2. Population change calculated for all the trajectories in the (a) Rh and (b) isoRh model systems. Generation of each form is counted only after the product region in the ground state. The others are counted as “residual.” All the curves have already reached their respective asymptotes as shown.

the bathoRh ($\lambda_{\text{max}} = 570 \text{ nm}$) absorption maximum is reached and little change in the 570 nm absorption is observed at later times. In this simulation, this instant would correspond to the time when the bathoRh population in the S_0 well reaches maximum. The population of bathoRh reaches maximum at 187 and 344 fs for Rh and isoRh, respectively, as shown in Table 3, as photoisomerization periods. The periods are reasonably reproduced with a slight underestimation. The underestimation would be mainly due to the overestimation of excitation energies. In addition, the underestimation in isoRh may be due to the lack of a barrier in the excited state, which was suggested by experiment.^{15,53} The chosen QM treatment would not adequately reproduce the barrier in the S_1 state of isoRh, resulting in a faster twist of the active dihedral. Another possibility may be insufficient description of surrounding protein by the present MM force set.

To obtain the excited-state time constants, we fitted the change in the excited-state population (see Figure S3, SI) with an appropriate exponential decay function. The resultant lifetimes of the excited state are 56 and 139 fs for Rh and isoRh, respectively. These would be reasonable estimates for fluorescence lifetimes. Kochendoerfer and Mathies reported that the fluorescence lifetime of Rh is a mere $50 \pm 20 \text{ fs}$, while that of isoRh is twice longer ($100 \pm 40 \text{ fs}$).⁵⁶ The time constants obtained are in reasonable agreement with the fluorescence lifetime although we did not calculate fluorescence lifetime directly.

One may attribute the reaction time scale and efficiency to the difference in excess energy stemming from the energy difference between the Franck–Condon point in the excited state and the MECI, near which transitions take place. However, the difference in excess energy cannot explain the dissimilarity in reaction time as discussed in section of MECIs in Energetics of the Systems.

In our gas-phase PSB model calculation of the 9-*cis* retinal,² a 10 kcal mol⁻¹ barrier was found to have slowed down the 9-*cis* retinal photoisomerization to a time scale of 665 fs. Higher levels of theory, larger active space, and inclusion of dynamic electron (CASPT2(10,10)/6-31G)^{57,58} placed this barrier at 1.7 kcal mol⁻¹.²³ However, in this QM/MM calculation, a barrier was not found. Thus, if we were to speculate, even a tiny barrier would have slowed down the photoisomerization in this simulation by trapping the trajectories in the excited state and yield a quantitatively accurate time scale although the attempt is currently beyond our scope because this would require a more accurate, time-consuming treatment of the QM region.

Time Evolution of the Energy Difference and Coherence in Rhodopsin. In rhodopsin, coherent vibrational motion of the photoproduct was observed in femtosecond pump–probe experiments by Wang et al.⁵⁹ Isorhodopsin isomerization, on the other hand, transient absorption measurements, did not reveal the coherence, resulting in a much slower dynamics and a significantly lower quantum yield.¹²

We examined the time evolution of the energy difference between the excited state and the ground state for the (a) Rh and (b) isoRh trajectories, which is shown in Figure 3 (see also Figure S4 for comparison with the in vacuo calculations, SI). Note that, in Figure 3, when the relevant trajectory is on the excited (ground) potential energy surface, the energy difference is taken to be positive (negative) on the vertical axis. An important feature in the plot of Figure 3a is a uniform oscillation of the energy difference throughout the relaxation in

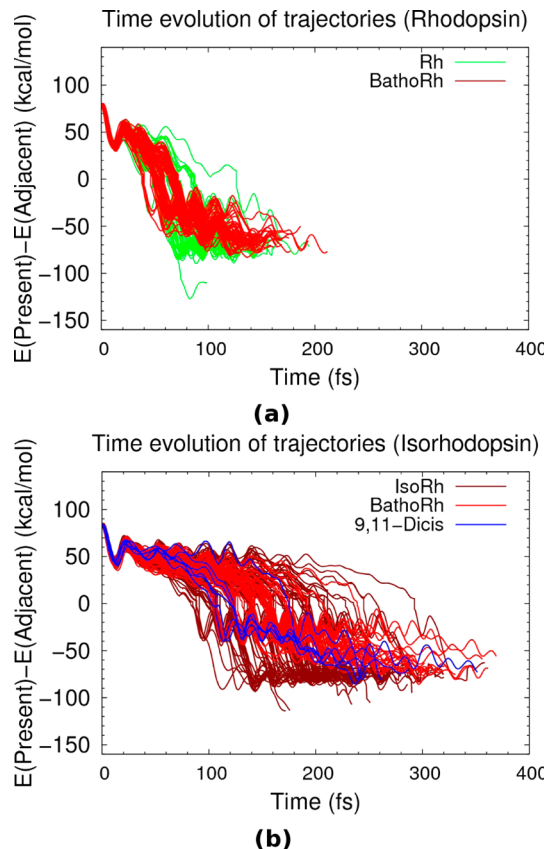


Figure 3. Time evolution of the signed energy difference between the ground state and the first excited state for each trajectory in the (a) Rh and (b) isoRh photoisomerization. Note that when the relevant trajectory is on the excited (ground) potential energy surface, the energy difference is taken to be positive (negative).

Rh, whereas a variety of trajectories are revealed in the isoRh case (Figure 3b). This uniformity is consistent with the computational result for Rh by Hayashi et al.²⁰

The more uniformity of the trajectories in Rh than in isoRh is also revealed in the standard deviations of spent time shown in Table 4. The standard deviations of time spent both in the S_1 and S_0 states for Rh are 12 and 20 fs, which are much less than those (36 and 32 fs) for isoRh. Table 4 also shows faster dynamics in Rh than in isoRh both in S_1 and S_0 . It takes 60 and 148 fs on average from excitation to nonadiabatic transition for Rh and isoRh and 71 and 92 fs after the transition to the products. The reaction in Rh is essentially finished after 130 fs, before any significant vibrational dephasing can occur.

The uniformity of the trajectories suggests the persistence of vibrational coherence of the Rh although the present classical treatment of nuclei except for transitions cannot describe the

quantum effects directly. Semiclassical treatment of nuclei is needed for an accurate description of the coherence in general, but it would be claimed that the present classical treatment give a plausible picture of the coherence in Rh, consistent with the experimental observation.

A larger degree of collective motion is noted in the isoRh photoisomerization in Figure 3b, something that is totally absent in the opsin-free 9-cis retinal simulation (see Figure S4(b2), SI). This should be attributed to the surrounding protein and the reduction of the excited-state barrier in the QM/MM calculation. The previous opsin-free calculation for 9-cis retinal²³ did not show a two-step relaxation mechanism although the mechanism was revealed in a similar simulation for 11-cis retinal²² (see Figure S4, SI).

Another prominent feature in Figure 3 is the oscillation of the energy difference in the ground state for both cases. The oscillation signifies the formation of a ground-state metastable intermediate that persists for some time before the ground-state photoproduct is finally formed. The energy difference oscillates between 10 and 40 kcal mol⁻¹ in the ground state for Rh as well as isoRh. For Rh and isoRh trajectories, an intermediate persists within 50–110 fs and 100–200 fs from excitation before reaching the most stable form in the ground state, respectively.

From Table 4, we have also found that the time-delaying feature of the isoRh photoisomerization originates mainly from the excited-state dynamics. When bathoRh forms, it spends 42% (58 fs) and 56% (148 fs) of reaction time for Rh and isoRh. Hence, the slower reaction is mainly due to the dynamics in the excited state in spite that we have found no finite barrier in the isoRh excited-state PES at the present level of theory.

Figure 4a and b shows the diagram of the active twist angle and the length of the active bond for five typical trajectories for Rh and isoRh, respectively. Fast and straightforward dynamics in Rh is illustrated in Figure 4a, whereas a rather complicated excited-state dynamics in a back-and-forth manner is evident in the isoRh case in Figure 4b. Thus, for Rh, the fast and straightforward dynamics in the excited state would be responsible for the coherence, higher quantum yield, and shorter reaction time. For isoRh, on the other hand, the complicated, back-and-forth dynamics in the excited state leads to slower and less efficient isomerization.

The complicated behaviors in trajectories seen in isoRh indicates the trajectories are greatly disturbed mainly by opsin. This opsin perturbation will be discussed in subsection Opsin Effects. The disturbance would be the origin that slows down the dynamics resulting in vibrational decoherence to take place before the reaction is finished although we cannot exclude the possibility that a barrier in the excited state, which is experimentally suggested, is also responsible for the slow dynamics.

Table 4. Averages and Standard Deviations of Time (fs) that Trajectories Spent in Each Electronic State

photoproducts	reactants					
	Rh(11-cis)			isoRh(9-cis)		
	S_1	S_0	total	S_1	S_0	total
overall	60 ± 12 (46%)	71 ± 20 (54%)	130 ± 24	148 ± 36 (62%)	92 ± 32 (38%)	239 ± 47
bathoRh(all-trans)	58 ± 9 (42%)	79 ± 20 (58%)	137 ± 24	148 ± 26 (56%)	116 ± 39 (44%)	263 ± 46
isoRh(9-cis)	not generated	not generated	not generated	150 ± 40 (66%)	77 ± 15 (34%)	227 ± 42
Rh(11-cis)	61 ± 14 (50%)	61 ± 15 (50%)	122 ± 21	not generated	not generated	not generated
9,11-di-cis-Rh	not generated	not generated	not generated	124 ± 26 (46%)	143 ± 32 (54%)	267 ± 49

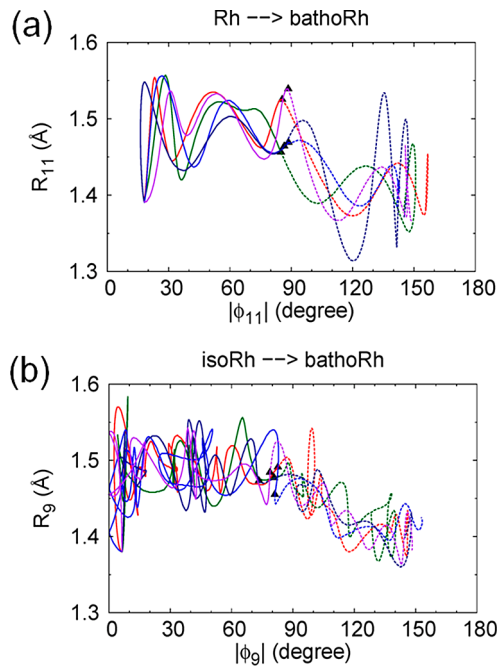


Figure 4. Change in length of the active bond $-C(n)-C(n+1)-$ against the absolute value of the dihedral angle $C(n-1)-C(n)-C(n+1)-C(n+2)$ for five typical (a) Rh and (b) isoRh trajectories leading to the all-trans form.

Time Evolution of Length and Angle of the Twisting Bond. Shown in Figure 5 are the plots of the time evolution of the active dihedral ϕ_{11} in Rh and ϕ_9 in isoRh for all the trajectories (see also, Figure S5, SI, for comparison with the trajectories in vacuo). Clearly seen in Figure 5a is the lack of access of trajectories to a clockwise twist in ϕ_{11} in addition to rapid change to -90° , where MECIs are located. In the case of

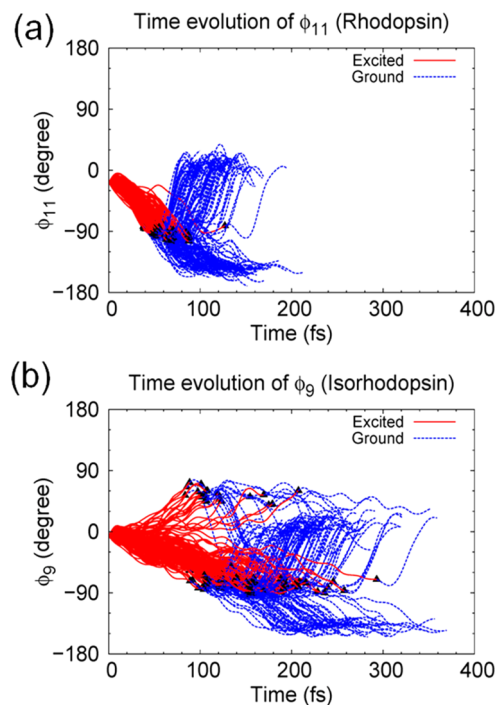


Figure 5. Time evolution of the dihedral angle for the twisting bond (active angle) for the (a) Rh and (b) isoRh systems.

isoRh, 13% of trajectories are initiated by a clockwise twist of ϕ_9 in the excited state. In this case, isoRh is mainly regenerated in the ground state, although a small portion of 9,11-di-cis-Rh is generated. Thus, all of the bathoRh photoproducts are formed via a counterclockwise twist of the active dihedral, be it ϕ_{11} or ϕ_9 . This obviously hindered isomerization is due to the constraints offered by the opsin environment, especially by the amino acid residues close to the binding pocket. In contrast, in the PSB simulations, both the clockwise and the counterclockwise twists of the active dihedrals take place (cf. Figure 6, ref 2; see also Figure S5(b2), SI). The comparison of Rh in Figure 5a with isoRh in Figure 5b reveals that the slower twist in isoRh in the excited state. This is another evidence of slower dynamics in the excited state for isoRh.

Shown in Figure S6 (SI) are plots of the length of the active bond R against the energy difference between the ground and excited states for typical (a) Rh and (b) isoRh trajectories. In all cases, R is stretched at the excited state and is typically of single-bond order upon transition. The bond length then oscillates around a single-bond order for some time, forming a metastable ground-state intermediate, before eventually regaining double-bond character and relaxing to a ground-state minimum. Such a mechanism has been observed in the photoisomerization of the PSB of 11-cis retinal.²² Without the protein environment, the PSB of 9-cis retinal does not appear to form a metastable intermediate in the ground state as the relaxation there occurs in a single step.²³

Motion of the Retinal Backbone. Shown in Figure 6 are plots of the time-dependent behavior of the dihedral angle of the retinal backbone atoms for typical trajectories. Analyzing the plots would give us an idea of how the chromophore reacts, in a structural sense, upon excitation and subsequent relaxation. One graph is generated per trajectory and we show one representative trajectory for successful/failed to produce bathoRh for Rh/isoRh in Figure 6.

All the trajectories exhibit so-called crankshaft or asynchronous bicycle pedal isomerization mechanism both for Rh and isoRh. Crankshafts and bicycle pedals rotate in a synchronous direction in real life, but the twists in Rh and isoRh are in the opposite directions each other. Thus, we propose a new term for this twist: "wring-a-wet-towel" motion. This is because when one wrings a wet towel, one twists the left-hand and the right-hand in the opposite direction to each other. It would be more suitable to use "wring-a-wet-towel" motion for the twists of ϕ_{11} and ϕ_9 in Rh and isoRh.

For Rh, all the trajectories are initiated by a counterclockwise twist of the active $-C11=C12-$ bond and a clockwise twist of the $-C9=C10-$ bond. The change of ϕ_9 and ϕ_{11} for Rh trajectories are rather monotonous in terms of the rotation of the ϕ_9 and ϕ_{11} centers. When the photoexcitation of Rh produces bathoRh in Figure 6(a1), the rotation of ϕ_{11} in the counterclockwise direction is accompanied by ϕ_9 clockwise twist first, but ϕ_9 turns to the opposite, counterclockwise direction and eventually back to 180° . When Rh is regenerated in Figure 6(a2), both the ϕ_9 and ϕ_{11} centers reverse their twist direction and go back to their initial configuration immediately after hopping to the ground state for majority of the trajectories.

In the formation of the bathoRh photoproducts from isoRh in Figure 6(b1), the active $-C9=C10-$ dihedral rotates in the counterclockwise direction although the twist direction is sometimes reverted temporarily into the clockwise direction. This reversion occurs much more often in isoRh trajectories,

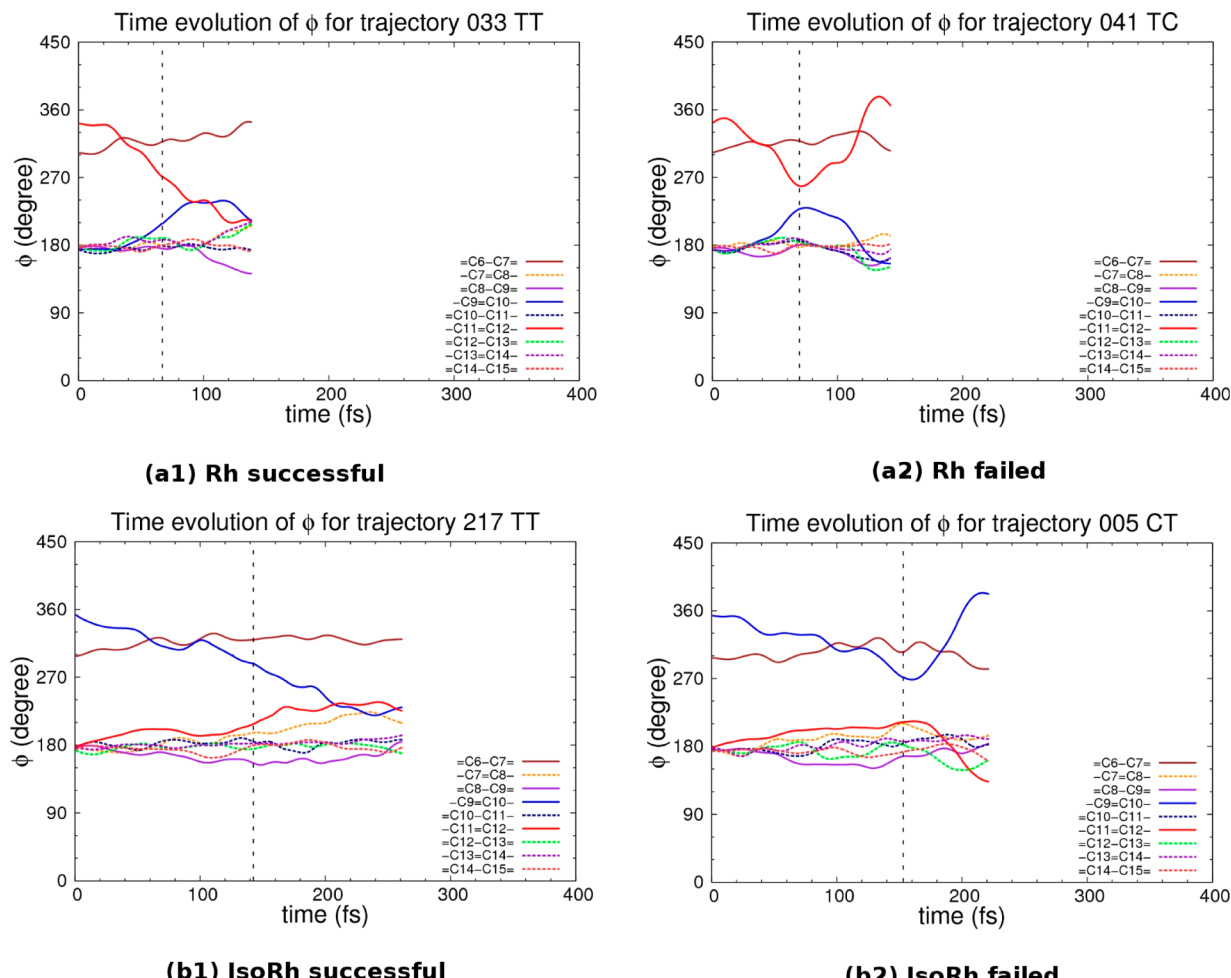


Figure 6. Time evolution of dihedral angles of the chromophore carbon backbone in typical trajectories. We chose one successful and one failed isomerization trajectories for the (a) Rh and (b) isoRh systems. The vertical dashed line shows the time when transition occurs.

indicating a hindered dynamics that is more of a rule rather than an exception in the isoRh case. At the same time, the $-C_{11}=C_{12}-$ dihedral is twisted in the opposite, clockwise direction and with temporary reversions in direction while maintaining an overall clockwise rotation. Eventually, the $-C_{11}=C_{12}-$ dihedral rotates back to the *trans* conformation via a counterclockwise twist. All the bathoRh photoproducts are generated in this manner. The regeneration of isoRh in Figure 6(b2) is also characterized by a counterclockwise-clockwise twist in ϕ_9 and ϕ_{11} , respectively, but both dihedrals rotate back to their original conformation. For a small number of trajectories that regenerate isoRh (9%), the rotations are in the opposite direction: clockwise twist of ϕ_9 and counterclockwise twist of ϕ_{11} .

All of the 9,11-di-*cis*-Rh isomers are generated through the ϕ_9 -clockwise and ϕ_{11} -counterclockwise twist in the excited state (not shown in Figure 6). In this isomerization, eventually the 11-position of the *trans* form is converted to the *cis* form and the 9-position returns to a *cis* configuration shortly after transition to the ground state.

Let us define here the associate angle as the other angle than the active angle for two angles which are relevant for the wring-a-wet-towel motion. For Rh and isoRh, the associate angles are ϕ_9 and ϕ_{11} as the active angles are ϕ_{11} and ϕ_9 , respectively. Using these definitions, we can summarize the results as follows. (1) All the trajectories show the wring-a-wet-towel

motion regardless of products. (2) For all the trajectories in Rh as well as most of trajectories in isoRh, the active angle twists in the counterclockwise direction and the associate angle twists in the clockwise direction. Only exception is a small portion of trajectories of isoRh (13%), where the active angle twists in the clockwise direction and the associate angle twist in the counterclockwise direction.

Geometries and Angle Velocities at the Transition Point.

In Figure 7, we have plotted the dihedral angle of the active twist angle ϕ_n against its angular speed $d\phi_n/dt$ at the instance of hopping for all trajectories to determine whether the angle and/or angular speed influence the stereochemistry of the resulting photoproduct (see also, Figure S7 for comparison with the *in vacuo* calculations, SI). Table 5 lists the averages and standard deviations for angular speed. the positive/negative sign indicates clockwise/counterclockwise rotation in Table 5.

Photoproducts are expected to be governed by the twist speed in the MECI region associated with *cis-trans* isomerization likely to proceed successfully at high negative twist speeds, where the negative sign indicates the speed is in the counterclockwise direction, therefore, toward to bathoRh. In Rh, the average hopping twist speed of the trajectories producing bathoRh is $-32.0 \text{ rad ps}^{-1}$ while for those that go back to reactant Rh is only $-14.7 \text{ rad ps}^{-1}$. The result is consistent with the expectation above. The value of the active

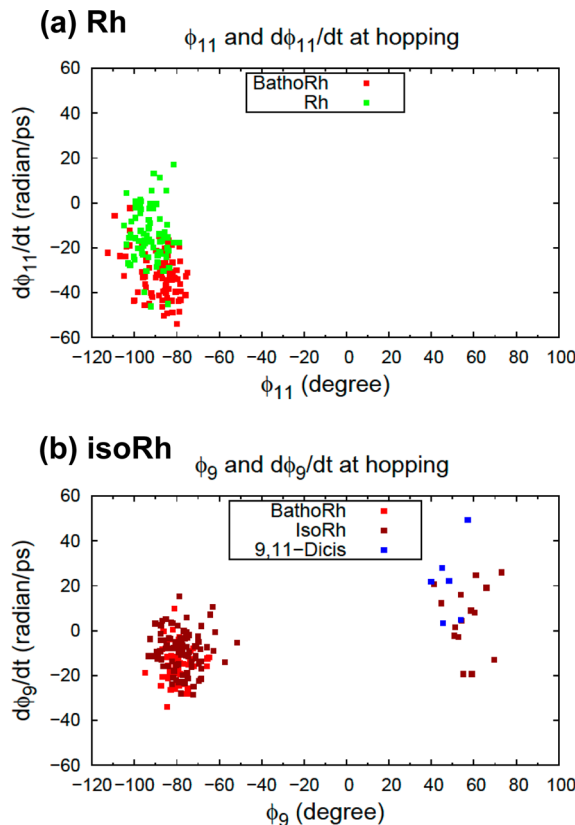


Figure 7. Diagrams for the active dihedral angle (ϕ_{11} for Rh and ϕ_9 for isoRh) and its speed at the instance of transition from the excited state to the ground state.

dihedral angle at the instance of hopping, on the other hand, has little influence on the resulting product.

When the twist speed is compared within trajectories where ϕ_9 is twisted counterclockwise, successful and failed hops occur at an average twist speed $d\phi_9/dt$ of -15.4 and -9.5 rad ps $^{-1}$. Thus, also in isoRh, larger twist speed of the active dihedral favors bathoRh generation, but the absolute value of 15.4 rad ps $^{-1}$ is less than half of that for Rh of 32.0 rad ps $^{-1}$. This would be one of consequences of complex and back-and-forth dynamics in the excited state of isoRh. From Figure 7a for Rh photoexcitation, the distribution of twist speed at the hopping for bathoRh formation is rather different from the twist speed distribution for Rh regeneration, whereas for isoRh photoexcitation, the corresponding difference is much less clear. The clearer separation in Rh than in isoRh would be

another consequence of the difference in dynamics between Rh and isoRh.

Schoenlein et al. attributed the slower reaction time and the lower yield in isoRh to slower speed along the reaction (twist) coordinate in the curve crossing area.¹² The present results are consistent with their attribution. The average absolute twist speed in Rh is 23.8 rad ps $^{-1}$ whereas the corresponding speed in isoRh is 11.6 rad ps $^{-1}$ for counterclockwise twists. However, the slower speed in the crossing area would not be the ultimate origin, but the complicated dynamics in excited state would be the prime cause of slower reaction time and the lower yield for isoRh.

When the active torsion coordinate is positive at the instance of transition in isoRh, the 9,11-di-*cis*-Rh is produced or isoRh is reproduced. In Table S, for 9,11-di-*cis*-Rh generation, the average twist speed of 21.5 rad ps $^{-1}$, whereas 5.6 rad ps $^{-1}$ for isoRh regeneration for clockwise twists. Thus, larger twist speed favors 9,11-di-*cis*-Rh for clockwise rotation of ϕ_9 in consistent with the expectation.

The effects of the opsin environment on the coordinate and twist speed of the active dihedrals is clarified when Figure 7 (with opsin) is compared to Figure S7, SI (without opsin). The most obvious effect is that the opsin environment enhances the dynamics by drastically reducing the probability of premature hopping, specially in the isoRh case (compare Figure S7(b1) with Figure S7(b2)), making transitions occur in the region near MECI. Another consequence due to the surrounding protein is the unidirectional photoisomerization for all (in the Rh case) or most (in the isoRh case) of trajectories, as discussed in section Time Evolution of Length and Angle of the Twisting Bond.

In Figure 8, the values of active/associate dihedral angles ϕ_9 and ϕ_{11} at the time of hopping are plotted (see also Figure S8, SI) together with the static paths from the Franck–Condon points to minima for products through MECI. Note that the static paths shown are not a calculated reaction path, but comes from smooth connection of the dots, but the actual reaction paths would not be very different. The minima (Franck–Condon points) and MECIs shown are obtained from the present calculations.

All the Rh trajectories go through only one region near MECI(Rh \rightarrow bathoRh) (shown as CI(R \rightarrow B) in Figure 8a) with $\phi_{11} \sim -90^\circ$ and slightly clockwise-twisted ϕ_9 . This MECI branches toward the formation of bathoRh and the regeneration of the reactant. The relaxation of the excited state of isoRh, on the other hand, goes through two MECI regions (Figure 8b). All the photoproducts bearing the all-*trans* chromophore are generated from isoRh through the region around MECI(isoRh \rightarrow bathoRh) (designated as CI(I \rightarrow B) in

Table 5. Average Twist Speed (rad ps $^{-1}$) at the Points where Transitions Take Place^a

photoproducts	reactants			
	Rh(11- <i>cis</i>)		isoRh(9- <i>cis</i>)	
	total ^b	counterclockwise twist of ϕ_9	clockwise twist of ϕ_9	total
overall	-23.8 ± 14.2	-11.6 ± 9.2	10.2 ± 16.7	-8.8 ± 12.7
bathoRh (all- <i>trans</i>)	-32.0 ± 10.4	-15.4 ± 8.1	not generated	-15.4 ± 8.1
isoRh(9- <i>cis</i>)	not generated	-9.5 ± 9.1	5.6 ± 14.9	-7.4 ± 11.4
Rh(11- <i>cis</i>)	-14.7 ± 12.1	not generated	not generated	not generated
9,11-di- <i>cis</i> -Rh	not generated	not generated	21.5 ± 16.9	21.5 ± 16.9

^aPositive/negative values correspond to clockwise/counterclockwise twist direction. ^bAll of the products from Rh is through counterclockwise twist of ϕ_{11} .

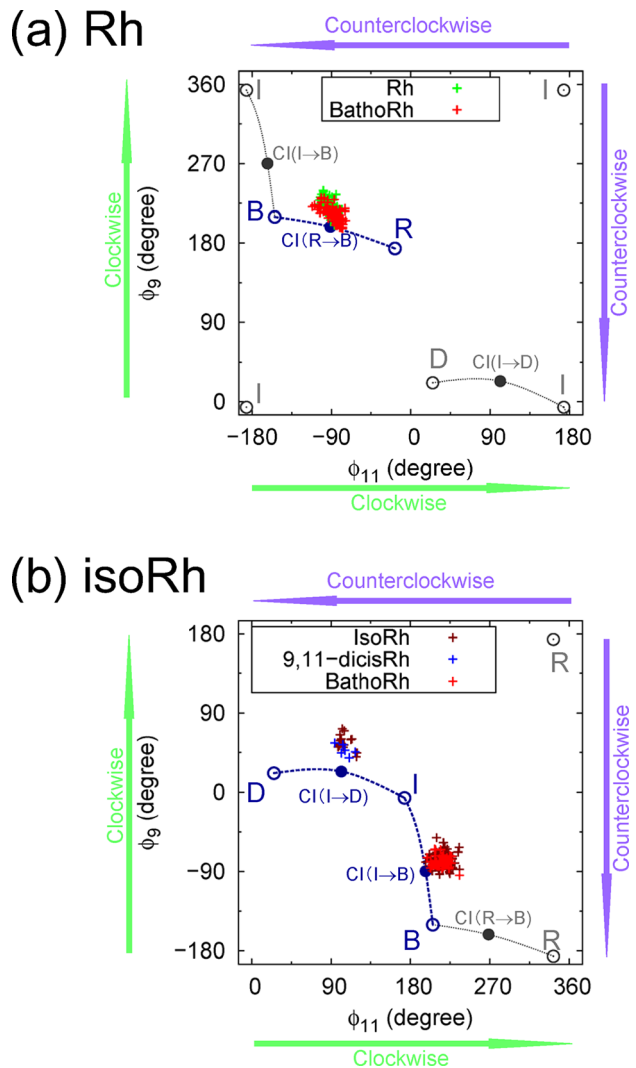


Figure 8. Diagram of the twist angles of $-C_{11}=C_{12}-$ (ϕ_{11}) and $-C_9=C_{10}-$ (ϕ_9) at the transition points. The transition points (+) are classified by products. The minima in the ground state (Franck-Condon points in the excited state; open circles) and MECIs (filled circles) obtained in the present calculations are also plotted in the diagram. The reactant and a product/products via MECI are connected with a smooth curved line to show a plausible reaction path although the path is not a calculated one. In each panel, the reactant Rh (a) or isoRh (b) is placed at the center of the panel. Blue points and paths are the relevant ones for each photoexcitation, whereas gray ones are less relevant ones. R = rhodopsin, I = isorhodopsin, B = bathorhodopsin, D = 9,11-di-cis rhodopsin, CI = MECI between them.

Figure 8b) with $\phi_9 \sim -90^\circ$ and a little clockwise-twisted ϕ_{11} . A large majority of the regenerated isoRh also goes through this region. On the other hand, the generation of the 9,11-di-cis-Rh photoproducts goes through another MECI region near MECI(isoRh \rightarrow 9,11-di-cis-Rh) (shown as CI(I \rightarrow D) in Figure 8b), one where ϕ_9 is slightly clockwise twisted and ϕ_{11} is around 90° . This MECI apparently branches toward the formation of the 9,11-di-cis-Rh and isoRh isomers as a few trajectories that regenerate isoRh also passes through this region.

The rate of reaction through the two MECI in isoRh is found to be significantly different. The reaction time is longer through MECI(isoRh \rightarrow BathoRh) than that through MECI(isoRh \rightarrow

9,11-di-cis-Rh). The average time is 233 and 188 fs, respectively. The difference is also revealed in the dissimilarity in the twist speed of ϕ_9 in Figure 1b. This difference in reaction time between the counterclockwise and clockwise twists in isoRh may be revealed in experimental observations.

The transition points for Rh are distributed in the upper side of the MECI($Rh \rightarrow$ BathoRh) (outside of the dashed blue arc in Figure 8a). This indicates the associate dihedral angle ϕ_9 at transitions is twisted more than ϕ_9 at the MECI. Also, the transition points for isoRh are distributed outside of the dashed blue arc for the two pathways. Thus, the wring-a-wet-towel motion is dynamically enhanced in comparison with the one expected statically from the MECI locations.

Strambi et al. found, from their reaction pathway analysis, that Rh and isoRh relax along a common excited-state potential energy valley starting from opposite ends,²⁴ employing a diagram corresponding to the upper-left part of Figure 8a (or the lower-right part of Figure 8b). Nonetheless, the present simulation shows neither direct production of isoRh from Rh photoexcitation nor production of Rh from the isoRh excitation. We have not found an MECI between Rh and isoRh, either, as described in subsection Energetics of the Systems. The present simulation indicates that, in Rh, the MECI($Rh \rightarrow$ bathoRh) funnels all trajectories to the ground state to produce bathoRh or reproduce Rh. In isoRh, also, MECI(isoRh \rightarrow bathoRh) funnels all trajectories to the ground state to yield bathoRh or isoRh again. Thus, no trajectories would go through the common valley to reach another MECI neither from the Rh photoexcitation nor from the isoRh excitation. Thus, the common valley in the excited state (around point B in S_1 in Figure 8a or b) would not play a significant role on real dynamics in Rh and isoRh, although the valley gives an insight to topology of the S_1 surface.

Compared to similar topology plots of their bare PSB counterparts (in Figure S8 of SI; Figure 11, ref 1 and Figure 10, ref 2), transition points concentrate more near the MECI, that is, the protein funnels trajectories to the MECI region. The protein may keep large the energy gap between the excited state and the ground state except for the MECI region. Thus, premature transitions occur much less often with the opsin effect, especially in the isoRh case.

To check the accuracy in transition point distribution with the present treatment of CASSCF(6,6)-ME, we estimated energy differences at the CASSCF(12,12)-EE at twenties of the present transition points. The energy differences were 22.1 and 26.0 kcal mol⁻¹ in average for twenties of trajectories, whereas the corresponding original energy differences are 2.6 and 3.2 kcal mol⁻¹. This difference between CASSCF(6,6)-ME and CASSCF(12,12)-EE suggests the present transition points are significantly different from those for CASSCF(12,12)-EE. However, the present CASSCF(6,6)-ME treatment has successfully reproduced the difference in reaction time and quantum yield between rhodopsin and isorhodopsin. Thus, the present treatment would describe the qualitative feature of potential energy surfaces reasonably for a comparative study of rhodopsin and isorhodopsin.

Opsin Effects. We now summarize and extend discussion on opsin effect by comparing QM/MM-optimized structures and MD trajectories with results in vacuo. The time scale is essentially captured without the protein environment, but the explicit consideration of the surrounding protein corrects the direction of the photoisomerization and slightly affects the photoisomerization period. Thus, the role of the amino acid

residues that envelope the chromophore is mainly to ensure that the photoisomerization proceeds in the right direction and optimize the production of the all-*trans* photoproduct, whereas the tendency to photoisomerize upon absorption of a photon is intrinsic to the chromophore itself by nature's design. Also, the isoRh formation is totally blocked from Rh and vice versa. Furthermore, the opsin causes transitions to take place near the MECIs.

Here, we examine the shape of the chromophore pocket to understand hindrance effect on PSB movements in the photoisomerization dynamics. Shown in Figure 9, clipped to

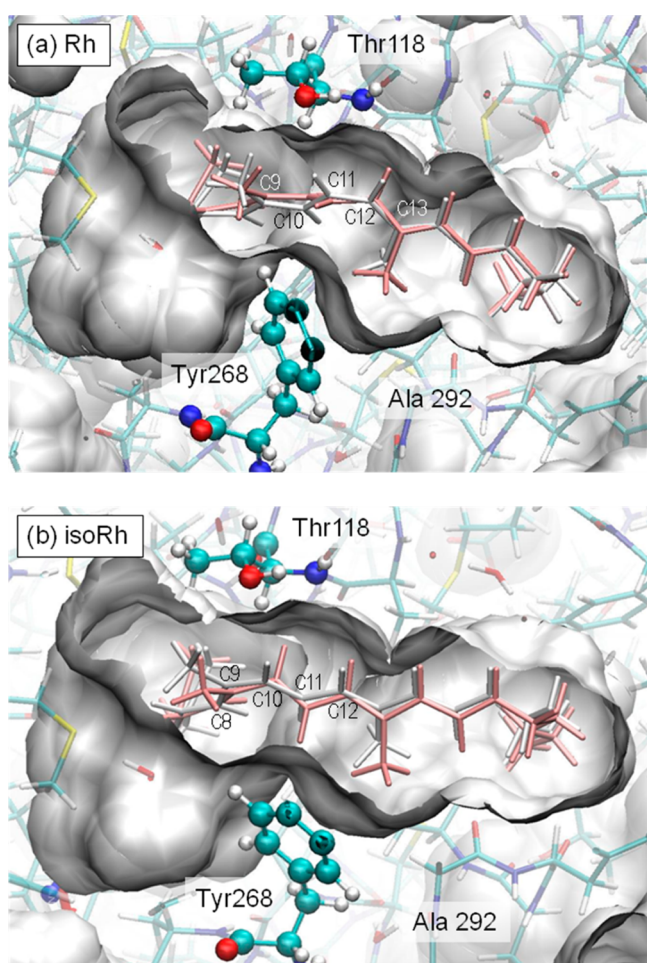


Figure 9. Superimposed structures of the ground-state optimized geometry (gray) and geometry at the MECI (pink) for the (a) Rh and (b) isoRh case. Also shown is the opsin pocket that contains the chromophore. The pocket surface is the overlapped envelope of amino residues surrounding retinal chromophore, which is generated using the ground-state optimized geometry wherein the retinal chromophore is artificially removed. The graphics is generated by VMD.⁶⁵

best illustrate the most relevant spatial features, is the retinal pocket, some opsin residues close to the pocket with two stick-modeled PSB configurations in its stable ground-state and MECI geometry. The pockets for both Rh and isoRh are similar in shape. The most important feature for both pockets is a narrow space between Tyr 268 and Thr 118 near the =C8=C9=C10=C11= (ϕ_9) rotation center with the two residues coming as close as 7 Å to each other. Comparing the structures reveals the reason why Rh photoisomerization is easier: (1) the Rh isomerization is more space-saving than that of isoRh and

(2) the dihedral that needs to be twisted in the isoRh case (=C9=C10=) is situated within the narrow gap between Thr 118 and Tyr 268. Also, there is hardly any space for the C₉ methyl group to move as it is invariably displaced as a consequence of the rotation of the ϕ_9 center of isoRh. The ϕ_{11} rotation center in Rh, on the other hand, is situated within a relatively wide space and thus the rotation can proceed more easily.

Another feature of the pockets is a relatively large hollow space in between Tyr 268 and Ala 292 close to the C13 methyl group. The large space aids tremendously in the fast isomerization of Rh. In the cis-trans isomerization of the ϕ_{11} center, the C13 methyl group is displaced as a consequence and the space is large enough to accommodate this displacement.

Our previous gas-phase PSB simulations have unambiguously revealed that the Rh and isoRh photoisomerization stimulus have intrachromophore origins.^{22,23} For instance, in the case of Rh, steric repulsion between the hydrogen bonded to C10 (C10-H) and the C13 methyl group can easily drive the photoisomerization as suggested by other groups.^{12,60,61} In the isoRh case, hydrogen atoms bonded to the C8 and C11 in the 9-cis chromophore offers some steric strain to the =C8=C9=C10=C11= dihedral that can be relieved by *cis-trans* isomerization. The stimulus largely originates from intra-chromophore steric interactions although the dynamics can later fail, mainly twist in a wrong way, without the modulation offered by the opsin residues resulting in more amount of undesired photoproducts as we have seen in the PSB calculations.

Delange et al. showed from spectroscopic measurements that methyl substitution to the 10-position dramatically slowed down the kinetics of the Rh photocascade.⁶² Their result is consistent with the present picture since the substitution would increase the steric hindrance from Try 268 from Figure 9a. Creemers et al. observed downfield proton NMR ligitation shift for the hydrogen atoms bonded to C16, C17, and C19 and hydrogen atoms in the ionone ring and claimed the existence of global, nonspecific steric interactions between PSB and the opsin.⁶³ The global, nonspecific steric hindrance surely influences the dynamics, but the narrow gap between Tyr 268 and Thr 118 would be mainly responsible for slow and back-and-forth dynamics in isoRh.

Liu et al. suggested that the peptide oxygen of Cys 187 (Cys187-O), which is one of the closest atoms to PSB, would assist the large movement of C12 during photoisomerization by repulsive interaction.⁶⁴ Sekharan et al. pointed out the distance between C12 and the Cys 187-O was larger in isoRh and claimed that the larger distance is consistent with less effective isomerization in isoRh.¹⁹ We also find a larger distance of 3.33 Å in isoRh than 3.26 Å in Rh in the optimized geometry in the ground state. The difference in the distance may be related to efficiency of the isomerization although the detailed analysis of the relevant forces would be necessary.

Breakdown of Weiss-Warshel Model. Weiss and Warshel proposed a model for *cis-trans* photoisomerization in 1979.³⁷ In their paper, the relationship between the quantum yield and transition probability is represented by

$$Y = \frac{1-f}{2-\theta} \quad (1)$$

where f is the fraction of molecules that never reach the crossing region and θ is the transition probability per passing over the crossing region. For Rh, we would be able to put $f=0$

because the transition takes place almost at $70^\circ < |\phi_{11}| < 110^\circ$. Now we get

$$Y = \frac{1}{2 - \theta} \quad (2)$$

They assumed that a trajectory goes back and forth around the crossing point in the excited state. In their scheme, if the transition takes place when the trajectory goes forth, the product is generated and if it does when the trajectory goes back, the ground state reactant is regenerated. To check if their scheme is applicable to the present systems, we counted how many trajectory make turns before transitions for Rh. If their argument is correct, the number of turns should be strongly correlated to the compound generated: if the number of turns is even (odd), it should result in the product (reactant). It is found, however, that the ratio of the generated compounds expected from the number of turns was 58.3%, which means that the correlation is weak because 50% corresponds to no correlation. This weak correlation is seen from the distribution of transition points with respect to $d\phi_{11}/dt$ in Figure 7a. In the Weiss–Warshel model, if $d\phi_{11}/dt$ were negative (positive), the product is essentially bathoRh (Rh). The simulation results, however, shows that roughly $d\phi_{11}/dt \gtrsim -20 \text{ rad ps}^{-1}$ yields bathoRh, while $d\phi_{11}/dt \lesssim -20 \text{ rad ps}^{-1}$ leads to Rh shown in Figure 7a. Furthermore, the correlation would be less as the momentum component is smaller in the direction of the active twist angle (ϕ_{11} or ϕ_9). In the present CAS treatment, the excess energies in the crossing area would be overestimated, and the momentum component along the twist angles also would be. Thus, in the actual situation, the correlation would be less than the simulation results of 58.3%.

Moreover, it is found that the transition probability for the first passing over the transition region (corresponding to no turns) is 0.95. When $\theta = 0.95$ is substituted in eq 2, $Y = 0.95$, which is totally different from 0.52, the quantum yield value from the present simulation.

Thus, it is concluded that the model by Weiss and Warshel of photoisomerization is not applicable to rhodopsin in spite of the fact that they bore rhodopsin in mind, as shown in Figure 3 in their paper. It is found that the branching ratio after the transition at the first passing is critically important, not the transition probability per passing during multiple passing in the Rh photoisomerization. This situation would come from the qualitative feature of potential energy surfaces of Rh as well as the present treatment of nonadiabatic transitions. The fundamental picture, therefore, would not change even if more sophisticated approach is employed in the part of electronic structure computations. From this conclusion, the model based on the branching ratio at the transition would be desirable for rhodopsin photoisomerization.

CONCLUSION

The *cis*–*trans* photoisomerization dynamics of rhodopsin and isorhodopsin was simulated using the ZN-QM/MM-TSH scheme that we have proposed. Comparisons were made between rhodopsin and isorhodopsin as well as between species in opsin and those in vacuo. The experimental higher quantum yield and faster isomerization period in Rh than those in isoRh were reproduced semiquantitatively in this simulation although the small barrier in S_1 for isoRh was not reproduced. We included only an essential part of PSB as the QM region and used mechanical embedding for the opsin to reproduce the

results, which suggests that the long-range charge effect play a minor role in dynamics.

The dynamics in Rh is straightforward and fast whereas the dynamics in isoRh is complex and in a back-and-forth manner. The coherence observed in experiments for Rh would be the consequence of the fast and straightforward dynamics. The complex dynamics for isoRh is mainly due to the narrower space near the active dihedral angle ϕ_9 , which is the active dihedral in isoRh, than the space around ϕ_{11} , which is the active dihedral in Rh. The narrower space is created mainly by Thr 118 and Tyr 268 in opsin. Because rhodopsin's and isorhodopsin's tendency to photoisomerize have an intrachromophore origin, the opsin environment is not required for isomerization to start and/or to proceed. The opsin, on the other hand, confines the photoisomerization in one direction and funnels transitions into the vicinity of MECI although the confinement in isoRh is incomplete, leading to a byproduct. The confinement and funneling effects enhance the production of bathorhodopsin photoproduct. The opsin environment is also totally blocks simultaneous twisting of ϕ_9 and ϕ_{11} for Rh as well as isoRh. Thus, the equilibration between Rh and isoRh upon irradiation observed in the experiments^{8,9} would be via bathoRh because Rh photoexcitations do not generate isoRh, vice versa. The common valley in S_1 between MECI(Rh → bathoRh) and MECI(isoRh → bathoRh)²⁴ would not play a significant role on real dynamics in Rh or isoRh although the valley gives an insight into the PES topology in S_1 .

The difference in excess energy cannot explain the origin of the difference in rate and efficiency between Rh and isoRh. The difference in pretwist^{17,18} plays only a small role, as described in our previous paper.²³

Photoexcitation of Rh gives only one product, bathoRh, whereas isoRh leads to a 9,11-di-*cis* form in addition to bathoRh. The selectivity of the product for Rh in addition to faster response time and higher quantum yield would be main biological reasons why living creatures have selected 11-*cis* retinal as chromophore for Rh instead of 9-*cis* form in the evolution process, as suggested in our previous paper.³⁶

We have proposed term “wring-a-wet-towel” motion for the twists of the active and associate angles for Rh and isoRh. All the trajectories show the wring-a-wet-towel motion regardless of products for Rh as well as isoRh. For almost all the trajectories in Rh and isoRh, the active angle twists in the counterclockwise direction and the associate angle twists in the clockwise direction. The wring-a-wet-towel motion is dynamically enhanced in comparison with the one expected from the MECI locations.

We have argued against the Weiss–Warshel model where the active twist angle oscillates around the crossing region in the excited state and the direction of the twist angle momentum uniquely determines the products.³⁷ The present simulation has revealed that the branching ratio after transition plays a crucial role.

We calculated 162 trajectories in Rh and isoRh, but this number of trajectories might not be enough to give accurate statistical results, especially when a small quantum yield is calculated. Massively parallel computations are a trend in supercomputers at present. The supercomputers would be suitable for trajectory calculations, in which no communications among computation nodes are needed during the simulation, although the time duration of each trajectory varies. Thus, calculations of thousands trajectories for biological systems are expected to be routinely carried out in the near future.

The ZN-QM/MM-TSH treatment of the photoisomerization dynamics of isoRh and Rh provides us with quantum yields and lifetimes of near-quantitative to quantitative quality. Coupled with a more rigorous description of a wider QM region, the scheme would yield results more in agreement with experimental measurements. Thus, we have demonstrated excellent applicability of the scheme for the simulation of the excited-state relaxation dynamics of large biological molecules. The ZN-QM/MM-TSH scheme is a promising approach with a wide range of possible applications.

ASSOCIATED CONTENT

Supporting Information

Voluminous figures that illustrate the difference between the previous opsin-free simulations and this calculation. This material is available free of charge via the Internet at <http://pubs.acs.org>.

AUTHOR INFORMATION

Corresponding Author

*E-mail: ishida@fukui.kyoto-u.ac.jp.

Present Address

[§]Department of Chemistry, De La Salle University—Manila, 2401 Taft Avenue, 1004 Manila, Philippines.

Notes

The authors declare no competing financial interest.

ACKNOWLEDGMENTS

The computations were performed using Research Center for Computational Science, Okazaki, Japan, and Research Institute for Information Technology of Kyushu University. This research is supported by Grant-in-Aids for Scientific Research (C) 20608003, (C) 24550021, and (B) 19350013 from the Japan Society for the Promotion of Science (JSPS). W.C.C. acknowledges the postdoctoral research fellowship at the Kyoto University Fukui Institute for Fundamental Chemistry and the Kyoto University Start-Up Grant for Young Scientists.

REFERENCES

- (1) Boll, F. *Am. J. Med. Sci.* **1878**, *151*, 190.
- (2) Hubbard, R.; Wald, G. *J. Gen. Physiol.* **1952**, *36*, 269.
- (3) Yoshizawa, T.; Kito, Y. *Nature* **1958**, *182*, 1604.
- (4) Wald, G.; Brown, P. K.; Gibbons, I. R. *J. Opt. Soc. Am.* **1963**, *53*, 20.
- (5) Collins, F. D.; Morton, R. A. *Biochem. J.* **1950**, *47*, 18.
- (6) Wald, G.; Brown, P. K.; Hubbard, R. *Proc. Natl. Acad. Sci. U.S.A.* **1955**, *41*, 438.
- (7) Yoshizawa, T.; Wald, G. *Nature* **1963**, *197*, 1279.
- (8) Schick, G. A.; Cooper, T. M.; Holloway, R. A.; Murray, L. P.; Birge, R. R. *Biochemistry* **1987**, *26*, 2556.
- (9) Hug, S. J.; Lewis, J. W.; Kliger, D. S. *J. Am. Chem. Soc.* **1988**, *110*, 1998.
- (10) Schoenlein, R. W.; Peteanu, L. A.; Mathies, R. A.; Shank, C. V. *Science* **1991**, *254*, 412.
- (11) Peteanu, L. A.; Schoenlein, R. W.; Wang, Q.; Mathies, R. A.; Shank, C. V. *Proc. Natl. Acad. Sci. U.S.A.* **1993**, *90*, 11762.
- (12) Schoenlein, R. W.; Peteanu, L. A.; Wang, Q.; Mathies, R. A.; Shank, C. V. *J. Phys. Chem.* **1993**, *97*, 12087.
- (13) Dartnall, H. J. A.; Goodeve, C. F.; Lythgoe, R. V. *Proc. R. Soc. A* **1936**, *156*, 158.
- (14) Kim, J. E.; Tauber, M. J.; Mathies, R. A. *Biochemistry* **2001**, *40*, 13774.
- (15) Hurley, J. B.; Ebrey, T. G.; Honig, B.; Ottolenghi, M. *Nature* **1977**, *270*, 540.
- (16) Fan, J.; Rohrer, B.; Moiseyev, G.; Ma, J. X.; Crouch, R. K. *Proc. Natl. Acad. Sci. U.S.A.* **2003**, *100*, 13662.
- (17) Okada, T.; Sugihara, M.; Bondar, A. N.; Elstner, M.; Entel, P.; Buss, V. *J. Mol. Biol.* **2004**, *342*, 571.
- (18) Nakamichi, H.; Buss, V.; Okada, T. *Biophys. J.* **2007**, *92*, L106.
- (19) Sekharan, S.; Sugihara, M.; Weingart, O.; Okada, T.; Buss, V. *J. Am. Chem. Soc.* **2007**, *129*, 1052.
- (20) Hayashi, S.; Tajkhorshid, E.; Schulten, K. *Biophys. J.* **2009**, *96*, 403.
- (21) Frutos, L. M.; Andruniów, T.; Santoro, F.; Ferré, N.; Olivucci, M. *Proc. Natl. Acad. Sci. U.S.A.* **2007**, *104*, 7764.
- (22) Ishida, T.; Nanbu, S.; Nakamura, H. *J. Phys. Chem. A* **2009**, *113*, 4356.
- (23) Chung, W. C.; Nanbu, S.; Ishida, T. *J. Phys. Chem. A* **2010**, *114*, 8190.
- (24) Strambi, A.; Coto, P. B.; Frutos, L. M.; Ferre, N.; Olivucci, M. *J. Am. Chem. Soc.* **2008**, *130*, 3382.
- (25) Maseras, F.; Morokuma, K. *J. Comput. Chem.* **1995**, *16*, 1170.
- (26) Svensson, M.; Humbel, S.; Froese, R. D. J.; Matsubara, T.; Sieber, S.; Morokuma, K. *J. Phys. Chem.* **1996**, *100*, 19357.
- (27) Polli, D.; Altoe, P.; Weingart, O.; Spillane, K. M.; Manzoni, C.; Brida, D.; Tomasello, G.; Orlandi, G.; Kukura, P.; Mathies, R. A.; Garavelli, M.; Cerullo, G. *Nature* **2010**, *467*, 440.
- (28) Persico, M.; Granucci, G.; Inglese, S.; Laino, T.; Toniolo, A. *J. Mol. Struct.: THEOCHEM* **2003**, *621*, 119.
- (29) Schafer, L. V.; Groenhof, G.; Boggio-Pasqua, M.; Robb, M. A.; Grubmuller, H. *PLoS Comput. Biol.* **2008**, *4*, e1000034.
- (30) Warshel, A.; Chu, Z. T. *J. Phys. Chem. B* **2001**, *105*, 9857.
- (31) Ciminelli, C.; Granucci, G.; Persico, M. *Chem. Phys.* **2008**, *349*, 325.
- (32) Ruckenbauer, M.; Barbatti, M.; Sellner, B.; Muller, T.; Lischka, H. *J. Phys. Chem. A* **2010**, *114*, 12585.
- (33) Weingart, O.; Altoe, P.; Stenta, M.; Bottoni, A.; Orlandi, G.; Garavelli, M. *Phys. Chem. Chem. Phys.* **2011**, *13*, 3645.
- (34) (a) Tully, J. C. *J. Chem. Phys.* **1990**, *93*, 1061. (b) Hammes-Schiffer, S.; Tully, J. C. *ibid.* **1994**, *101*, 4657. (c) Parahdekar, P. V.; Tully, J. C. *ibid.* **2005**, *122*, 094102.
- (35) (a) Craig, C. F.; Duncan, W. R.; Prezhdo, O. V. *Phys. Rev. Lett.* **2005**, *95*, 163001. (b) Hyeon-Deuk, K.; Madrid, A. B.; Prezhdo, O. V. *Dalton Trans.* **2009**, *45*, 10069. (c) Duncan, W. R.; Craig, C. F.; Prezhdo, O. V. *J. Am. Chem. Soc.* **2007**, *129*, 8528. (d) Madrid, A. B.; Hyeon-Deuk, K.; Prezhdo, O. V. *ACS Nano* **2009**, *3*, 2487.
- (36) Chung, W. C.; Nanbu, S.; Ishida, T. *Chem. Lett.* **2011**, *40*, 1395–1397.
- (37) Weiss, R. M.; Warshel, A. *J. Am. Chem. Soc.* **1979**, *101*, 6131.
- (38) Frisch, M. J.; et al. *Gaussian 03*, revision C.02; Gaussian, Inc.: Wallingford, CT, 2004.
- (39) (a) Werner, H.-J.; Knowles, P. J. *J. Chem. Phys.* **1985**, *82*, 5053. (b) Knowles, P. J.; Werner, H.-J. *Chem. Phys. Lett.* **1985**, *115*, 259.
- (40) Hehre, W. J.; Ditchfield, R.; Pople, J. A. *J. Chem. Phys.* **1972**, *56*, 2257.
- (41) Cornell, W. D.; Cieplak, P.; Bayly, C. I.; Gould, I. R.; Merz, K. M.; Ferguson, D. M.; Spellmeyer, D. C.; Fox, T.; Caldwell, J. W.; Kollman, P. A. *J. Am. Chem. Soc.* **1995**, *117*, 5179.
- (42) Swope, W. C.; Andersen, H. C.; Berens, P. H.; Wilson, K. R. *J. Chem. Phys.* **1982**, *76*, 637.
- (43) Zhu, C. Y.; Nakamura, H. *J. Chem. Phys.* **1994**, *101*, 4855.
- (44) Zhu, C. Y.; Nakamura, H. *J. Chem. Phys.* **1994**, *101*, 10630.
- (45) Zhu, C. Y.; Nakamura, H. *J. Chem. Phys.* **1995**, *102*, 7448.
- (46) Nakamura, H. *J. Theor. Comput. Chem.* **2005**, *4*, 127.
- (47) Nakamura, H. *Adv. Chem. Phys.* **2008**, *138*, 95.
- (48) Mayne, H. R. In *Dynamics of Molecules and Chemical Reactions*; Wyatt, R. E., Zhang, J. Z. H., Eds.; Marcel Dekker, Inc.: New York, 1996; p 589.
- (49) Nakamichi, H.; Okada, T. *Angew. Chem., Int. Ed.* **2006**, *45*, 4270.
- (50) Randall, C. E.; Lewis, J. W.; Hug, S. J.; Bjorling, S. C.; Eisner-Shanas, I.; Ottolenghi, M.; Sheves, M.; Friedman, N.; Kliger, D. S. *J. Am. Chem. Soc.* **1991**, *113*, 3473.
- (51) Palczewski, K. *Annu. Rev. Biochem.* **2006**, *75*, 743.

- (52) Yoshizawa, T.; Shichida, Y.; Matuoka, S. *Vision Res.* **1984**, *24*, 1455.
- (53) Birge, R. R.; Einterz, C. M.; Knapp, H. M.; Murray, L. P. *Biophys. J.* **1988**, *53*, 367.
- (54) Hubbard, R.; Kropf, A. *Proc. Natl. Acad. Sci. U.S.A.* **1958**, *44*, 130.
- (55) Trehan, A.; Liu, R. S. H.; Shichida, Y.; Imamoto, Y.; Nakamura, K.; Yoshizawa, T., Y. *Bioorg. Chem.* **1990**, *18*, 30–40.
- (56) Kochendoerfer, G. G.; Mathies, R. A. *J. Phys. Chem.* **1996**, *100*, 14526.
- (57) Werner, H.-J. *Mol. Phys.* **1996**, *89*, 645.
- (58) Ditchfield, R.; Hehre, W. J.; Pople, J. A. *J. Chem. Phys.* **1971**, *54*, 724.
- (59) Wang, Q.; Schoenlein, R. W.; Peteanu, L. A.; Mathies, R. A.; Shank, C. V. *Science* **1994**, *266*, 422.
- (60) Ganter, U. M.; Gärtner, W.; Siebert, F. *Eur. Biophys. J.* **1990**, *18*, 295.
- (61) Gartner, W.; Ternieden, S. *J. Photochem. Photobiol. B* **1996**, *33*, 83.
- (62) DeLange, F.; Bovee-Geurts, P. H. M.; VanOostrum, J.; Portier, M. D.; Verdegem, P. J.E.; Lugtenburg, J. *Biochemistry* **1998**, *37*, 1411–1420.
- (63) Creemers, A. F. L.; Bovee-Guerts, P. H. M.; DeGrip, W. J.; Lugtenburg, J.; de Groot, H. J. M. *Biochemistry* **2004**, *43*, 16011–16018.
- (64) Liu, R. S. H.; Hammond, G. S. *Acc. Chem. Res.* **2005**, *38*, 396.
- (65) Humphrey, W.; Dalke, A.; Schulten, K.; Molec, J. *Graphics* **1996**, *14*, 33–38, <http://www.ks.uiuc.edu/research/vmd/>.
- (66) Shichi, H. *Biochemistry* **1970**, *9*, 1973.
- (67) Rudzki, J. E.; Peters, K. S. *Biochemistry* **1984**, *23*, 3843.